

Ultrafast structural dynamics of the photo-cleavage of protein hybrid nanoparticles -Supporting Information

I. SMALL ANGLE X-RAY SCATTERING

Small angle x-ray scattering probes density inhomogeneities in the sample, in the range of nanometers to hundreds of nanometers, depending on the geometry and the instrumental resolution [1–3]. The atomic (crystallographic) ordering is neglected and the scattering cross section is given by

$$S(Q) = r_e^2 N \left| \int_V \Delta\rho(r) \exp(-iQr) dr \right|^2 \quad (1)$$

$$= r_e^2 N \cdot V^2 \Delta\rho^2 F^2(Q) \times C(Q) \quad (2)$$

with the $S(Q)$ being scattered intensity per space angle element versus the incident x-ray flux, the classical electron radius r_e , $Q = 4\pi/\lambda \cdot \sin(2\Theta/2)$ the scattering vector with x-ray wavelength λ and scattering angle 2Θ and the electron density difference $\Delta\rho(r)$ of the scattering objects. The spatial integral over the object is called particle form factor. When assuming compact gold particles of spherical shape and radius R an analytical function can be given for the form factor:

$$F(Q, R) = 3[\sin(QR) - (QR) \cos(QR)]/(QR)^3, \quad (3)$$

which is a function that shows oscillations at Q positions, which scale with the inverse of the particle size. In general as the particles are not monodisperse, the form factor is convoluted by the size distribution function [4].

For the modeling of our system of a BSA shell on the particles the structure factor of a core-shell system was used:

$$S(Q) = \left[\frac{4\pi}{3} (\rho_{shell} - \rho_{water}) R_{shell}^3 \cdot F(Q, R_{shell}) \right] +$$

$$\begin{aligned}
& + \frac{4\pi}{3} (\rho_{part.} - \rho_{shell}) R_{part.}^3 \cdot F(Q, R_{part.})^2, \\
F(Q, R_i) & = 3[\sin(QR_i) - (QR_i) \cdot \cos(QR_i)] / (QR_i)^3.
\end{aligned} \tag{4}$$

The expression $F(Q, R_i)$ is the form factor for a homogeneous sphere of radius R_i , where i is given by the radii of particle, resp. the outer protein shell, with electron density ρ_i .

A model independent quantity for the (difference) scattering yield is the Porod invariant:

$$P = \int_0^\infty S(Q) Q^2 dQ = 2\pi^2 \Delta\rho^2 r_e^2 \Phi(1 - \Phi) \tag{5}$$

as it allows to derive the the global scattering length density contrast $\Delta\rho$ change after laser excitation without the need for assumptions on particle shape and size. Φ denotes the filling fraction of the particles.

II. WIDE ANGLE SCATTERING

Wide angle scattering probes the spatial correlations between all atoms present. Most of the atoms in the present system are disordered, which gives rise to broad features in reciprocal space. The gold nanoparticles are polycrystalline, therefore distinct powder peaks are visible reflecting the gold fcc lattice.

Scattering from disordered systems such as water can be described by a scalar function depending only on the momentum transfer Q . The Fourier transform of the electron density distribution can be collapsed on the so-called Debye equation, where the intensity S can be expressed relative to the primary intensity in absolute units (Warren, 1990).

$$S_{eu}(Q) = \sum_m \sum_n f_m(Q) f_n(Q) \frac{\sin(Q \cdot R_{mn})}{Q \cdot R_{mn}} \tag{6}$$

with the amplitudes formed by the atomic scattering functions $f_{m,n}$ and the pairwise distance R_{mn} in between two atoms, which display a positional correlation. The $\sin x/x$ function contains the structural information on the molecular arrangement. In dense disordered systems

a second level of positional correlation can be separated, owing to a stiff molecular structure but disordered intermolecular positions. The intensity distribution is multiplied by a structure factor, which reflects the intermolecular statistical correlations. A consequence of the intermolecular correlation is the low scattering intensity at low Q and prominent correlation peaks of nearest or next-nearest neighbors. If a detector without energy discrimination is used to collect the diffracted signal additional contributions from inelastic processes will be added. The most prominent effect stems from the so-called Compton scattering. It is found to be in good approximation independent from structural properties and can be given quantitatively:

$$S(Q) \propto Z - \sum_{n=1}^Z f_{electron}^2(Q) \quad (7)$$

Phenomenological expression for the elements have been listed by Pálincas [5] and Hajdu [6]. It should be noted, that the absolute intensity of the scattering solutes can be expressed relative to the measured (and scaled) intensity from the solvent. This is important for an absolute estimation of the scattering yield of the protein molecules. The protein are modeled with the Debye function in eq. 6. The atom positions are obtained from the Protein data bank entry for the human serum albumin analog and computed into a scattering curve using the program Crysol by D. Svergun [7]. From this data a structureless SAXS curve has been subtracted, which possesses the same radius of gyration and density. By this procedure a transition from a folded protein to a random coil of the same extension is mimicked.

In the time resolved data difference scattering is derived by subtracting the non-excited signal from the scattering signal of an excited suspension, such that only the excitation related contributions remain. While for the modeling of the SAXS signal and the protein scattering the respective scattering distributions are taken, the difference scattering from the solvent can be treated differently. It has been shown, that the difference scattering $\Delta S(Q)$ of thermally or photo-excited liquids can be explained by first derivatives with respect to temperature T , pressure p or volume V [8]. They scale linearly with T , p or V for small changes. Only two of

them are independent. It has been earlier shown, that the bubble formation process causes a compression of the bulk of the water phase, showing specific signatures of the function

$$\Delta S(Q) = dS(Q)/dp|_T \times \Delta p \quad (8)$$

Then the absolute amplitude of $\Delta S(Q)$ scales with the pressure rise and thus with the volume expansion (Δp) of the bubbles [9,10]. Specifically minima of $\Delta S(Q)$ around 1.75 and 3 \AA^{-1} and a maximum around 2.3 \AA^{-1} is expected. This can be seen for the highest fluence values in fig. 6 of the main article. As bubble sizes close to the nucleation threshold were small a larger contribution from the shift and reduction of powder scattering from the gold particles is seen.

III. PARTICLE CONJUGATION

We have compared the adsorption of bovine serum albumin directly onto the citrate covered particles and as well of particles with a buffer layer of mercaptosuccinic acid (MCSA). To a fixed volume of 100 ml nanoparticle suspension were added 0.8 ml of MCSA (10 mM) and after shaking for 2 minutes stepwise a small amount of BSA solution. At each step the optical extinction and dynamic light scattering were measured. Finally 12 ml of a 0.5 % NaCl solution was added to the extracted volume in order to induce aggregation of the nonligated particles.

The addition of NaCl destabilizes the electrostatic stabilization of the nanoparticles, which causes aggregation. The BSA layer, however, stabilizes the particles against aggregation by adding a steric repulsion to the interparticle interaction.

Optical spectroscopy is performed with a fiber spectrometer (Ocean Optics USB2000) and a fiber coupled light source (Ocean Optics). The suspensions were measured in disposable cuvettes with 4.5 mm optical path length (PMMA, semi-micro). The DLS apparatus is custom built, consisting in a 1.2 mW He-Ne laser (632 nm), a 90 ° scattering geometry, a fiber coupled

Avalanche Geiger module (SensL) and a multi-tau correlator (correlator.com). The nanoparticle suspension was placed in a standard 4 sided cuvette with 10 mm path length. Dynamic light scattering probes the temporal autocorrelation of the scattered light intensity $I(t)$ from the sample inhomogeneities. When diffusional motion is present the intensity autocorrelation g^2 :

$$g^2(Q, \tau) = \frac{\langle I(t)I(t + \tau) \rangle}{\langle I(t) \rangle^2} \quad (9)$$

will decay exponentially with correlation time τ with an exponent $\Gamma = q^2 D_h$ containing the diffusion constant D and the scattering vector Q . For spherical particles the hydrodynamic diameter D_h is calculated with the formula:

$$D_h = \frac{32\pi \cdot n_{liq}^2 \cdot kT}{3\eta \cdot \lambda^2} \times \sin \Theta \cdot \tau \quad (10)$$

with n_{liq} being the refractive index of the solvent, kT Boltzmann constant and temperature, η the dynamic viscosity of the solvent, λ the wavelength of the laser, Θ the scattering angle and τ the correlation time. Due to the high particle density the contrast in the autocorrelation function was limited to about 0.55, which still allowed to determine the correlation time with good precision within 2-5 minutes. Correlation spectroscopy has been shown to give size information for different nanoparticles, clustering [11] and particle hybridization [12,13]. The increasing coverage of nanoparticles with the protein is seen in the optical extinction as a red shift of the plasmon resonance. This is caused by an increase of the refractive index around the particles [14]. The correlation time in dynamic light scattering increases strongly, as the hydrodynamic diameter includes the immobilized protein shell. In Figs S1 and S2 the changes in extinction and hydrodynamic radius during the titration of the nanoparticle suspension with BSA are shown.

FIGURES

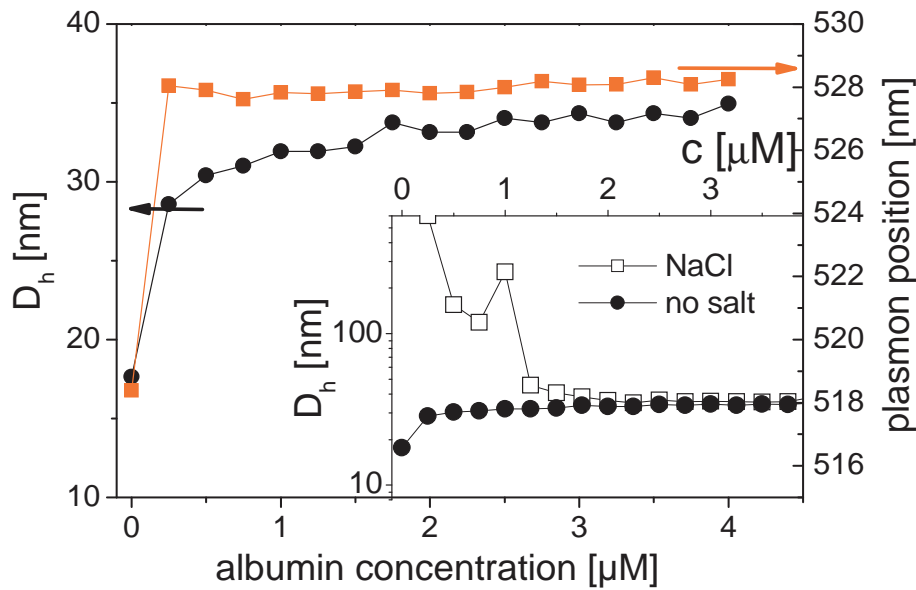


Figure S 1. Change of the plasmon peak position (red squares) and hydrodynamic diameter from DLS (black bullets) of the gold nanoparticles of 17 nm diameter as function of BSA concentration. The inset shows the hydrodynamic diameter of the particles before (black bullets) and after salt addition (open squares).

It is remarkable that the adsorption onto the pure citrate covered particles starts with an abrupt increase and then reaches final values slowly at about 3 μM BSA, while for the MCSA covered particles the adsorption is smoother and can be fitted with a Langmuir isotherm. In both cases a perfect stabilization against salt induced aggregation is reached at about 2 μM of BSA. We expect that in the case of citrate covered particles the van der-Waals interaction with BSA is stronger, so that a strong distortive adsorption of the BSA takes place, possibly by replacing the weakly bound citrate molecules. While a thin compressed layer can be formed at low BSA concentration a further addition of BSA either restructures the BSA layer or forms a second, more weakly bound layer. In the second case MCSA is bound covalently by a sulfur bond, so that it can act as spacer.

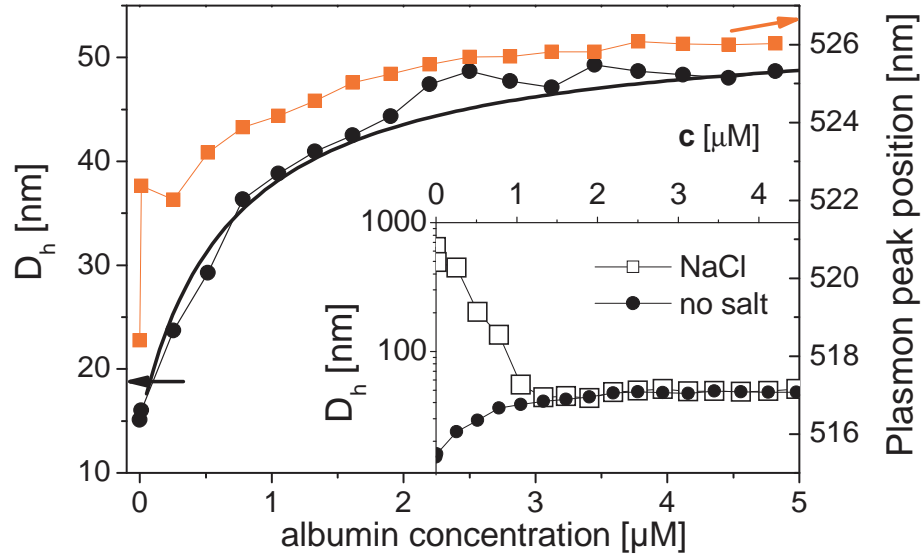


Figure S 2. Change of the plasmon peak position (red squares) and hydrodynamic diameter from DLS (black bullets) of the gold nanoparticles of 17 nm diameter as function of BSA concentration. The solid line is a fit according to the Langmuir adsorption equation (see text). The inset shows the hydrodynamic diameter of the particles before (black bullets) and after salt addition (open squares).

Brewer et al. [15] have analysed the BSA adsorption on citrate covered gold surfaces and nanoparticles. They found an electrostatic binding of BSA through the interaction of negative surface charges with cationic groups at the BSA surface (lysines). They find a maximum coverage of 3.7×10^{12} molecules/cm². Here the apparent hydrodynamic diameter is more than one presumed monolayer of BSA (assuming a size of $5.5 \times 5.5 \times 9$ nm³ [16]), which may stem from additional BSA adsorbed in a second layer or by the influence of dangling strands into the solution [12]. Irrespective of the applicability of the Langmuir adsorption we can fit an effective isotherm, which would give a maximum coverage of 1.6×10^{12} molecules/cm². When using a BSA size of $4 \times 4 \times 5$ nm³, as suggested by PDB data for human serum albumin (HSA) [17] one would obtain a maximum coverage of $3.2 \cdot 10^{12}$ molecules/cm², close to the values of Brewer et al. The rates of adsorption are indeed similar to the Brewer study $1.45 \pm 0.1 \mu M^{-1}$ compared to their value of $1.0 \mu M^{-1}$. Bilayers were also observed in the work by Kaufman et al. [16].

Further evidence for the BSA adsorption onto the gold particles comes from titration and

SAXS detection of the core-shell structure. These experiments have been performed at the cSAXS beamline at the Swiss Light Source (SLS) in Villigen (CH). The titration has been effectuated by a motorized syringe pump adding up to 10 ml of a 60 μM BSA solution to a volume of 100 ml gold particle suspension. While stirring a part of the volume is extracted continuously by a second syringe pump and flown through an x-ray capillary of 1 mm diameter (Hilgenberg). Small angle scattering of 9.5 keV x-rays was recorded on a pixellated hybrid detector (Pilatus, 2 megapixel) with exposures every two seconds.

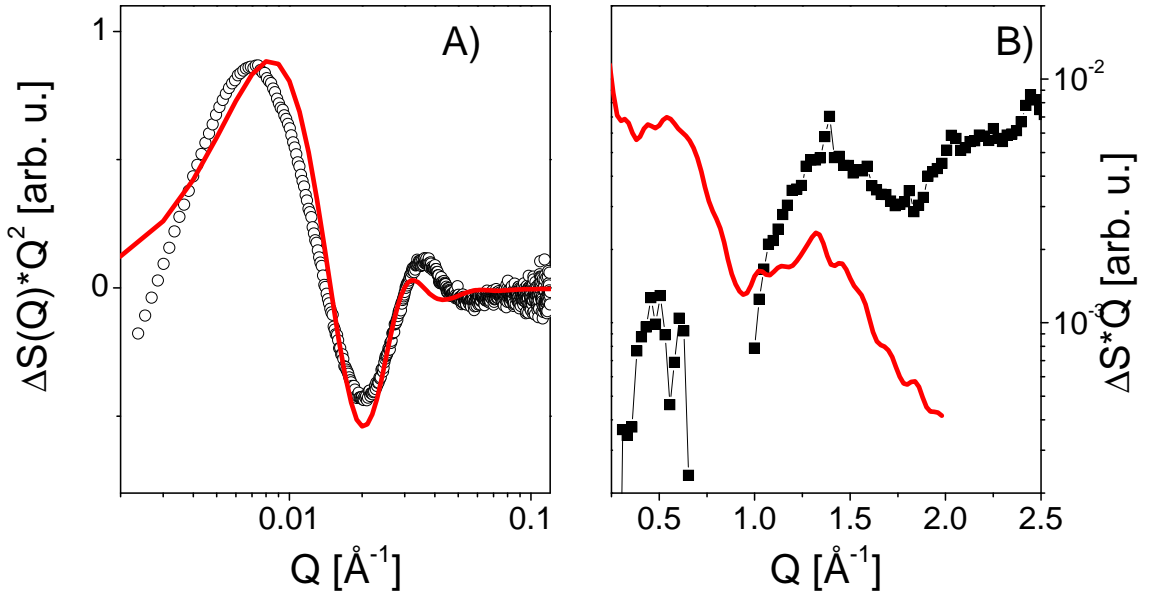


Figure S 3. Left: Difference $\Delta S(Q) \cdot Q^2$ of SAXS intensities of 16 nm gold particles after the BSA adsorption versus the unhybridized particles (dots) from a reference experiment at the . The full red line represents a fit with a core-shell model. Right: Difference $\Delta S(Q) \cdot Q^2$ of BSA adsorbed particles versus unhybridized particles during the photoexcitation experiment at ESRF. The full red line shows the atomic resolution model for the scattering of HSA.

The change in scattering $\Delta S(Q) = S(Q)_{BSA} - S(Q)_{bare}$ in Fig. S3 (left side) marks the end of the titration, when the change does not change any more with further addition of BSA. It shows characteristic undulations. A fit of these undulations reveals a BSA layer thickness of 9.3 nm, which is very close to a monolayer coverage in the model of Kaufman et al. [16]. The

(electron) density is 19 % higher than the water density.

In the wide angle scattering S3 (right side) the difference between the protein coated batch and bare nanoparticles shows the existence of the helix peak, while the exact match between theoretical curve and atomic model calculation (Crysol, HSA structure from PDB entry 1 BJ5) suffers from comparing different batches of gold particles.

A second proof for the survival of the secondary helical structure of the BSA upon adsorption on the gold particles can be deduced from ultraviolet circular dichroism measurements (UV-CD) of BSA in solution and adsorbed onto gold particles. In fig. S4 the CD of native BSA is compared to that of BSA on gold particles. The amplitude of the CD signature is unchanged irrespective of the binding of BSA (once electrostatically on citrate and once via activation of thiol bonds with Tris (2-carboxyethyl)phosphine hydrochloride TCEP). By heating the BSA-nanoparticle hybrid suspension to 70 °C the CD amplitude decays strongly (both for the TCEP and the electrostatically bound BSA), which proves thermal denaturation upon static heating.

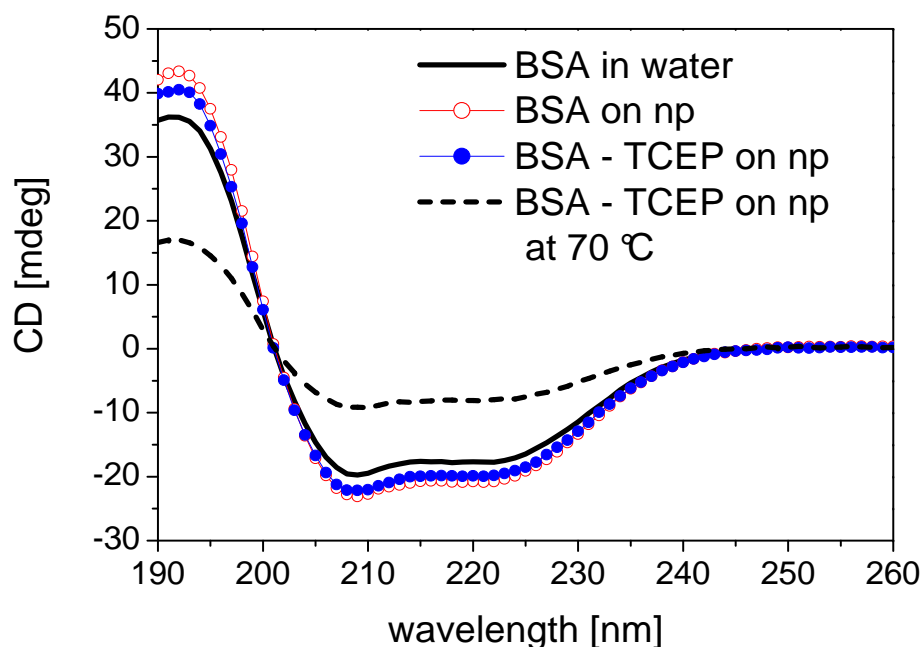


Figure S 4. UV circular dichroism spectra of BSA in solution, adsorbed onto the citrate coated gold particles and bound via thiol bond (TCEP) at room temperature and at 70 °C.

IV. RATE EQUATION FOR PROTEIN EXPULSION

The efficiency of protein expulsion from the nanoparticles is modeled by a dose-response curve, assuming the reaction probability RP of removing a certain amount of protein is given by a sigmoidal curve:

$$RP(\Delta T) = \frac{1}{\sqrt{2\pi\sigma^2}} \cdot \int_{-\infty}^{\Delta T} \exp(-(P(\Delta T') - P(\Delta T_{50}))^2/2\sigma^2) d\Delta T'$$

with the difference Porod invariant P, the 50 % RP at ΔT_{50} of 129 K and the width of the transition σ of 35 K.

REFERENCES

- [1] Guinier, A.; Fournet, G. **1955**, *Small-angle scattering of X-rays*, John Wiley & Sons, New York.
- [2] Warren, B. E. **1990**, *X-ray Diffraction, reprint*, Dover Publications, New York.
- [3] Dingenouts, N.; Bolze, J.; Pötschke, D.; Ballauff, M. **1999**, *Advances in Polymer Science* *144*, 1.
- [4] Foerster, S.; Timmann, A.; Konrad, M.; Schellbach, C.; Meyer, A.; Funari, S. S.; Mulvaney, P.; Knott, R. **2005**, *J. Phys. Chem. B* *109*, 1347.
- [5] Pálinkás, G. **1973**, *Acta Cryst. A* *29*, 10.
- [6] Hajdu, F. **1972**, *Acta Cryst. A* *28*, 250.
- [7] Svergun, D. I.; Koch, M. H. **2002**, *Curr. Opin. Struct. Biol.* *12*, 654.
- [8] Cammarata, M.; Lorenc, M.; Kim, T. K.; Lee, J. H.; Kong, Q. Y.; Pontecorvo, E.; Russo, M. L.; Schiró, G.; Cupane, A.; Wulff, M.; Ihee, H. **2006**, *J. Chem. Phys.* *124*, 124504.
- [9] Kotaidis, V.; Plech, A. **2005**, *Appl. Phys. Lett.* *87*, 213102.
- [10] Plech, A.; Kotaidis, V.; Lorenc, M.; Wulff, M. **2005**, *Chem. Phys. Lett.* *401*, 565.
- [11] Ciesa, F.; Plech, A.; Mattioli, C.; Pescatori, L.; Arduini, A.; Pochini, A.; Rossi, F.; Secchi, A. **2010**, *J. Phys. Chem. C* *114*, 13601.
- [12] Sperling, R. A.; Liedl, T.; Duhr, S.; Kudera, S.; Zanella, M.; Lin, C.-A. J.; Chang, W. H.; Braun, D.; Parak, W. J. **2007**, *J. Phys. Chem. C* *111*, 11552.
- [13] Rodríguez-Fernández, J.; Pérez-Juste, J.; Liz-Marzán, L. M.; Lang, P.-R. **2007**, *J. Phys. Chem. C* *111*, 5020.

- [14] Kreibig, U.; Vollmer, M. **1995**, *Optical Properties of Metal Clusters*, Springer, Berlin.
- [15] Brewer, S. H.; Glomm, W. R.; Johnson, M. C.; Knag, M. K.; Franzen, S. **2005**, *Langmuir* *21*, 9303.
- [16] Kaufman, E. D.; Belyea, J.; Johnson, M. C.; Nicholson, Z. M.; Ricks, J. L.; Shah, P. K.; Bayless, M.; Pettersson, T.; Feldoto, Z.; Blomberg, E.; Claesson, P.; Franzen, S. **2007**, *Langmuir* *23*, 6053.
- [17] Curry, S.; Mandelkow, H.; Brick, P.; Franks, N. **1998**, *Nat. Struct. Biol.* *5*, 827.